

Number Density of Bright Lyman-Break Galaxies at $z \sim 6$ in the Subaru Deep Field ¹

Kazuhiro SHIMASAKU ^{2,3}, Masami OUCHI ^{4,5}, Hisanori FURUSAWA ⁶ Makiko YOSHIDA ²,
Nobunari KASHIKAWA ⁷, Sadanori OKAMURA ^{2,3},

¹Based on data collected at the Subaru Telescope, which is operated
by the National Astronomical Observatory of Japan.

²Department of Astronomy, School of Science, The University of Tokyo, Tokyo 113-0033
Email (KS): shimasaku@astron.s.u-tokyo.ac.jp

³Research Center for the Early Universe, School of Science, The University of Tokyo, Tokyo 113-0033

⁴Space Telescope Science Institute, 3700 San Martin Drive, Baltimore, MD 21218, USA

⁵Hubble Fellow

⁶Subaru Telescope, National Astronomical Observatory of Japan, 650 N. A'ohoku Place, Hilo,
HI 96720, USA

⁷National Astronomical Observatory, Mitaka, Tokyo 181-8588

(Received 2005 December 19; accepted 2005 April 15)

Abstract

We report on the bright Lyman-break galaxies (LBGs) selected in a 767 arcmin² area of the Subaru Deep Field. The selection is made in the $i - z_R$ versus $z_B - z_R$ plane, where z_B and z_R are new bandpasses with a central wavelength of 8842Å and 9841Å, respectively. This set of bandpasses enables us to separate well $z \sim 6$ LBGs from foreground galaxies and Galactic cool stars. We detect 12 LBG candidates down to $z_R = 25.4$, and calculate the normalization of the rest-frame far-ultraviolet (FUV: $\simeq 1400\text{Å}$) luminosity function at $M_{\text{FUV}} = -21.6$ to be $\phi(-21.6) = (2.6 \pm 0.7) \times 10^{-5} \text{ mag}^{-1} \text{ Mpc}^{-3}$. This must be the most reliable measurement ever obtained of the number density of bright $z \sim 6$ LBGs, because it is more robust against both contamination and cosmic variance than previous values. The FUV luminosity density contributed from LBGs brighter than $M_{\text{FUV}} = -21.3$ is $(2.8 \pm 0.8) \times 10^{24} \text{ ergs s}^{-1} \text{ Hz}^{-1} \text{ Mpc}^{-3}$, which is equivalent to a star formation rate density of $(3.5 \pm 1.0) \times 10^{-4} M_{\odot} \text{ yr}^{-1} \text{ Mpc}^{-3}$. Combining our measurement with those at $z < 6$ in the literature, we find that the FUV luminosity density of bright galaxies increases by an order of magnitude from $z \sim 6$ to ~ 3 and then drops by 10^3 from $z \sim 3$ to the present epoch, while the evolution of the total luminosity density is much milder. The evolutionary behavior of bright LBGs resembles that of luminous dusty star-forming galaxies and bright QSOs. The redshift of $z \sim 3$ appears to be a remarkable era in the cosmic history when massive galaxies were being intensively formed.

Key words: galaxies: evolution — galaxies: high-redshift — galaxies: luminosity function, mass function — galaxies: photometry

1. Introduction

Over the last decade, selection of star-forming galaxies at high redshift using continuum breaks seen in their far-ultraviolet (FUV) spectra has been applied successfully to deep multi-color images taken with large telescopes. Thousands of galaxies beyond $z \sim 2$ have been detected by this method in two-color planes; galaxies selected in this way are called Lyman-break galaxies (LBGs). For instance, LBGs at $z \sim 4$ can be isolated from foreground objects (lower-redshift galaxies and Galactic stars) in the $B - R$ vs $R - i$ plane, since they have extremely red $B - R$ colors and relatively blue $R - i$ colors. Various properties of LBGs up to $z \sim 5$ have been discussed in detail based on photometric data and follow-up spectroscopy (e.g., Steidel et al. 1999; Papovich et al. 2001; Shapley et al. 2001, 2003; Giavalisco & Dickinson 2001; Porciani & Giavalisco 2002; Foucaud et al. 2003; Iwata et al. 2003; Ando et al. 2004; Ouchi et al. 2004a,b).

Very recently, several groups have made surveys of a similar galaxy population at $z \sim 6$ using ultra-deep imaging data taken with Hubble Space Telescope (HST) and 8m-class telescopes. Most of them search for galaxies red in $i - z$. Such ‘ i -dropout’ galaxies are likely star-forming galaxies at $z \sim 6$, since the continuum break of $z \sim 6$ galaxies falls into the i band. Systematic studies of galaxies at $z \sim 6$ and beyond are crucial not only for the understanding of the formation and early evolution of galaxies during and just after the reionization epoch of the universe, but also for the identification of objects which contributed to the reionization.

We begin with a brief summary of the previous studies on $z \sim 6$ galaxies. Fontana et al. (2003) made a multi-color Very Large Telescope (VLT) and HST imaging survey aiming at detecting $4.5 < z < 6$ galaxies. In their VLT data for an area of about 30 arcmin², 13 candidates with $Z_{\text{AB}} \leq 25 \text{ mag}$ were found based on photometric redshifts, among which four were at $5 < z \leq 6$. Dickinson et al.

(2004) detected in early Advanced Camera for Surveys (ACS) GOODS data of 316 arcmin² five $z \sim 6$ candidates with $i - z > 1.3$ down to $z \simeq 26$ mag. Stanway et al. (2003, 2004) detected eight and six i -dropout ($i - z > 1.5$) galaxies with $z \leq 25.6$ in public HST ACS data of the GOODS-South (146 arcmin² area) and the GOODS-North (200 arcmin²), respectively. Bouwens et al. (2003) detected 23 $z \sim 6$ galaxy candidates in two ACS Guaranteed Time Observation fields (46 arcmin² in total) down to $z \sim 27.3$ mag. A deeper survey was made subsequently by Bouwens et al. (2004a) for two Hubble Ultra Deep parallel fields; 30 i -dropouts ($i - z > 1.4$) were found over 21 arcmin² down to $z = 28.1$. Bouwens et al. (2004b) discussed the size evolution of galaxies up to $z \sim 6$ in the Hubble Ultra Deep Field (HUDF) and the Hubble Ultra Deep parallel fields. Yan, Windhorst, & Cohen (2003) found 30 $z \sim 6$ candidates brighter than $z \simeq 28$ mag in an ACS/WFC parallel field (10 arcmin²). Yan & Windhorst (2004) found 108 candidates with $z \leq 30.0$ mag in the HUDF (10.34 arcmin²). Bunker et al. (2004) also made a search in the HUDF, finding 54 candidates at $z < 28.5$ mag with $i - z > 1.3$. Many of the studies have reported a decrease in the FUV luminosity density of bright galaxies by a factor of $\approx 3 - 8$ from $z \sim 3$ to $z \sim 6$ (Dickinson et al. 2004; Giavalisco et al. 2004; Stanway et al. 2003, 2004; Bouwens et al. 2004a; Bunker et al. 2004), although Fontana et al. (2003) and Bouwens et al. (2003) obtained a roughly constant luminosity density over this redshift range. Measuring the number density of bright LBGs accurately is of great importance in discussing and modeling the formation and evolution of massive galaxies.

There are, however, two main uncertainties involved in the previous studies of bright $z \sim 6$ LBGs. First, selection of LBGs by a single $i - z$ color is likely to suffer from a significant amount of contamination, especially at bright magnitudes, since red galaxies at $z \sim 1 - 2$ and Galactic cool stars can be as red in $i - z$ as $z \sim 6$ LBGs. Removal of unresolved objects in a high-resolution HST image is an efficient way to reduce the contamination by cool stars. However, high-resolution imaging is not helpful to separate red $z \sim 1 - 2$ galaxies from LBGs. Near infrared (NIR) photometry is useful especially for discriminating LBGs from red galaxies. In the previous studies, however, NIR photometry was either limited to a very small sky area, or not deep enough to securely separate red galaxies from LBGs. Second, the areas surveyed in the previous $z \sim 6$ LBG papers are a few tens to a few hundreds arcminutes, the widest being 346 arcmin². This may not be sufficiently large when one recalls an extremely low surface density of bright LBGs (an order of $\sim 10^{-2}$ arcmin⁻²) and large cosmic variance in their volume density expected from observations of lower-redshift LBGs and biased galaxy formation models. Thus, wide-field and deep two-color imaging is essential for constructing a large and clean sample of $z \sim 6$ LBGs.

In this paper, we report on a survey of $z \sim 6$ LBGs which is aimed to overcome the two main uncertainties in the previous surveys. We apply for the first time a two-color selection to imaging data as wide as 767 arcmin².

We obtain a reliable value of the number density of bright $z \sim 6$ LBGs. By combining our value with those in the literature, we examine the evolution of the number density of bright LBGs over $3 < z < 6$ and discuss the formation of massive galaxies.

The plan of this paper is as follows. Section 2 explains the strategy of our survey. Section 3 describes the photometric data used in our analysis. Selection of $z \sim 6$ LBGs is made in §4. Section 5 is devoted to results and discussion, and a conclusion is given in §6. AB magnitudes are used in this paper. We assume a flat universe with $\Omega_0 = 0.3$, $\lambda_0 = 0.7$, and $H_0 = 70$ km s⁻¹ Mpc⁻¹.

2. Strategy of Our Survey

Our survey covered an area of 767 arcmin² of the Subaru Deep Field (SDF; Maihara et al. 2001). This wide survey area will considerably smooth out large-scale cosmic variance which will be probably at present at $z \sim 6$. Several observations have reported large cosmic variance for $z > 5$ galaxies. Bremer et al. (2004) found that the surface density of $z \sim 5$ galaxies varies considerably over areas comparable to a single ACS pointing. Shimasaku et al. (2003, 2004) reported large inhomogeneity of the sky distribution of Lyman α emitting galaxies at $z \sim 5$ on scales of 50 Mpc. At $z \sim 6$, a transverse comoving length of 50 Mpc corresponds to 20'. Hu et al. (2004) and Ouchi et al. (2005) also found a highly inhomogeneous spatial distribution of $\simeq 5.7$ Lyman α emitting galaxies on tens of Mpc scales. See Somerville et al. (2004) for a theoretical prediction for cosmic variance of high-redshift galaxies.

The bandpasses we use for two-color selection are i , z_B , and z_R . The z_B and z_R filters, which were designed by us for this purpose, divide the SDSS z band into two at 9500 Å. Figure 1 plots the effective response curves of the z_B and z_R bandpasses which include the filter transmission, CCD sensitivity, throughput of the optics of the Subaru Telescope, and atmospheric extinction at an airmass of 1.2. The central wavelength and FWHM of the z_B and z_R bandpasses are (8842Å, 689Å) and (9841Å, 537Å), respectively. These two bandpasses enable us to measure the slope of continuum emissions redward of Lyman α , which is crucial for discriminating $z \sim 6$ objects from $z \sim 1 - 2$ red galaxies and cool stars both of which have similar $i - z_R$ but redder $z_B - z_R$ colors (see §4).

We have another three advantages of using z_B and z_R . First is that we can measure reliably rest-frame UV continuum flux from z_R photometry. The continuum flux of $i - z$ selected LBG candidates is usually measured from their z -band magnitude. However, a recent study based on spectroscopic observation of an i -dropout galaxy at $z = 6.33$ suggests that a large fraction of i -dropout galaxies may have a strong Ly α emission (Nagao et al. 2004). If this is true, measurements of the continuum flux of $z > 6$ galaxies from z -band photometry would be biased high due to contamination from Ly α emission. A galaxy's Lyman α line does not enter the z_R bandpass as long as the galaxy is at $z < 6.7$.

Second, we can construct an LBG sample of a well-

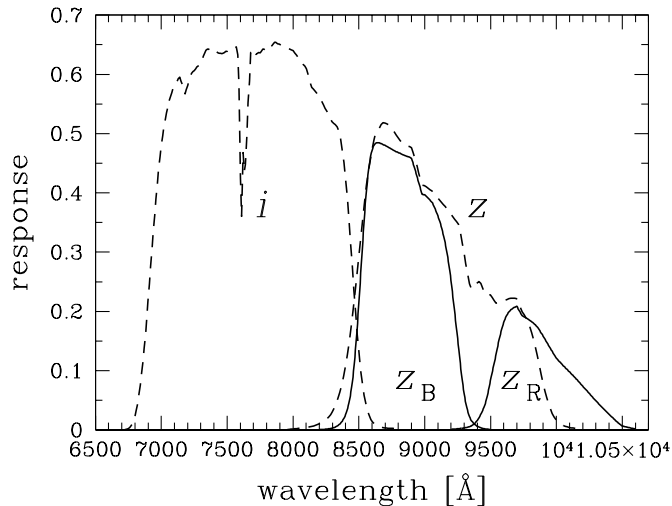


Fig. 1. Response functions of the z_B and z_R bandpasses (solid lines). The two dashed lines indicate the response of the i and z bands, respectively, of the Subaru/Suprime-Cam.

defined and relatively narrow redshift range thanks to $z_B - z_R$ color. As will be shown in §4, the $z_B - z_R$ value of star-forming galaxies increases rapidly with redshift at $z > 6$. Thus, selection of LBG candidates with $z_B - z_R$ color less than an appropriate value ($z_B - z_R = 0.7$ in this study) provides an LBG sample of a redshift distribution with a sharp upper limit, although the precise correspondence between $z_B - z_R$ and redshift varies with the intrinsic spectral shape of LBGs. This is important in calculating the comoving volume surveyed by our observation. In contrast, the selection function of a single $i - z$ color criterion is wide, having a long high-redshift tail.

Third, our $z \sim 6$ LBG sample is free from contamination by spurious objects near the detection limit of the z_R data. As will be seen in §4, one of our selection criteria for $z \sim 6$ LBGs is $z_B - z_R \leq 0.7$. Since the z_B data are deeper than the z_R data by about 0.7 mag, this criterion ensures that objects satisfying this criterion are detected in the z_B image as well. Fake objects in the z_R image which happen to exceed the detection flux are basically undetected in the z_B image, and thus will be eliminated by this criterion. Selection by $i - z$ color alone could be contaminated by spurious objects near the detection limit.

Table 1. Summary of the observational data.

Band	Exposure [min]	m_{lim}^*	Obs. date
z_B	85	26.2	2 July 2003
z_R	599	25.4	2 July 2003
			19, 20 March 2004
B	595	28.5	public
V	340	27.7	public
R	600	27.8	public
i	801	27.4	public
z	504	26.6	public
NB816	600	26.6	public
NB921	899	26.5	public

* 3σ limiting magnitudes on a $2''$ diameter aperture.

3. Data

3.1. z_B and z_R Imaging

We took deep z_B - and z_R -band imaging data of a $30' \times 24'$ area in the Subaru Deep Field (SDF) [$13^{\text{h}}24^{\text{m}}38.^{\text{s}}9$, $+27^{\circ}29'26''$ (J2000)] with the prime focus camera (Suprime-Cam; Miyazaki et al. 2002) mounted on the 8.2m Subaru telescope on 2003 July 2 and 2004 March 19 and 20. The image scale of Suprime-Cam is $0.''202$ per pixel. The exposure time was 85 min for z_B and 599 min for z_R ; we set a much longer exposure time for z_R , since the effective throughput of the z_R band is considerably lower than that of z_B due to the rapidly decreasing quantum efficiency of the CCDs toward longer wavelengths beyond 9500 Å. The individual CCD data were reduced and combined by IRAF and a data reduction software package for Suprime-Cam developed by Yagi et al. (2002) and Ouchi (2003). The combined images for individual bands were aligned and smoothed with Gaussian kernels so that the PSF sizes of the final images match those of the public images described in the next subsection. The final images after removal of low S/N regions near the edges of the field of view cover a contiguous 767 arcmin^2 area with a PSF FWHM of $0.''98$. Photometric calibration was made using the spectrophotometric standard star GD153 (Bohlin, Colina, & Finley 1995) taken on 2003 July 2 for both bandpasses. A summary of the data is given in Table 1.

3.2. Public Imaging Data

The SDF has deep, public Suprime-Cam data of seven bandpasses, B , V , R , i , z , NB816, and NB921, obtained in the Subaru Deep Field Project (Kashikawa et al. 2004). This project is a large program of Subaru Observatory to carry out a deep galaxy survey in a blank field in optical and NIR wavelengths to study distant galaxies. B , V , R , i , and z are standard Johnson and SDSS broad-bands, and NB816 and NB921 are narrow-bands whose central wavelength and FWHM are (8150 Å, 120 Å) and (9196 Å, 132 Å), respectively. The exposure times and limiting magnitudes of the public images are given in Table 1. We combine the i -band data with our z_B and z_R data to select LBGs at $z \sim 6$ in the $i - z_R$ vs $z_B - z_R$ plane. We also use

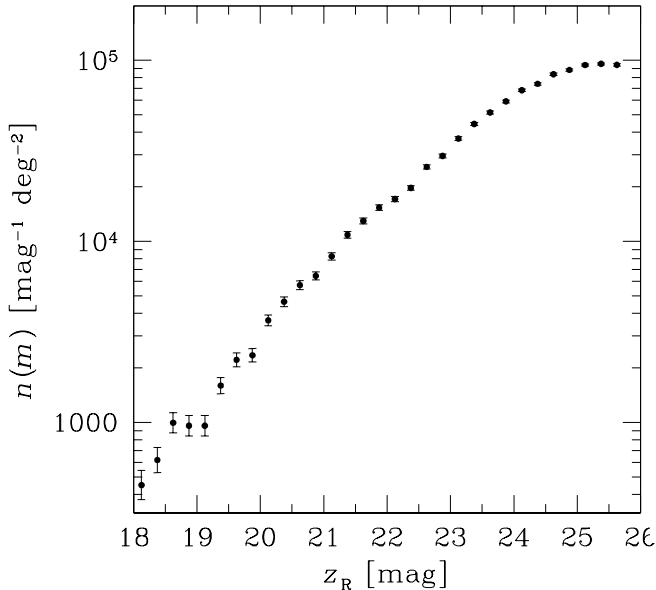


Fig. 2. Number counts of galaxies in the z_R band. Detection incompleteness has not been corrected. The error bars imply Poisson errors.

the B, V, R data to further remove foreground objects from the LBG sample.

3.3. Object Detection and Photometry

Object detection and photometry were made using SExtractor version 2.1.6 (Bertin and Arnouts 1996) on all nine images (z_B , z_R , and seven public images). The z_R -band image was chosen to detect objects. If more than 5 pixels whose counts were above the $2\sigma_{\text{sky}}$ were connected, they were regarded as an object. In total, 45,405 objects were detected down to $z_R = 25.4$ mag (3σ limiting magnitude). Figure 2 plots the number counts of objects detected in the z_R band, where stellar objects with the PSF shape brighter than $z_R = 23$ have been removed. For each object detected in the z_R image, a magnitude on a $2''$ -diameter aperture was measured for each passband to derive the colors of the object; we adopted for each object the same aperture among all passbands to ensure that the colors were measured correctly. We adopted MAG_AUTO for the total z_R magnitude.

4. Selection of $z \sim 6$ Lyman-break Galaxies

Figure 3 shows the selection of LBGs at $z \sim 6$ in the $i - z_R$ vs $z_B - z_R$ plane. The magenta curves in this figure indicate the tracks of young, star-forming galaxies at $z \geq 5$ with three dust extinction values, $E(B - V) = 0, 0.15, 0.50$; the filled squares on the curves correspond to $z = 6$. The

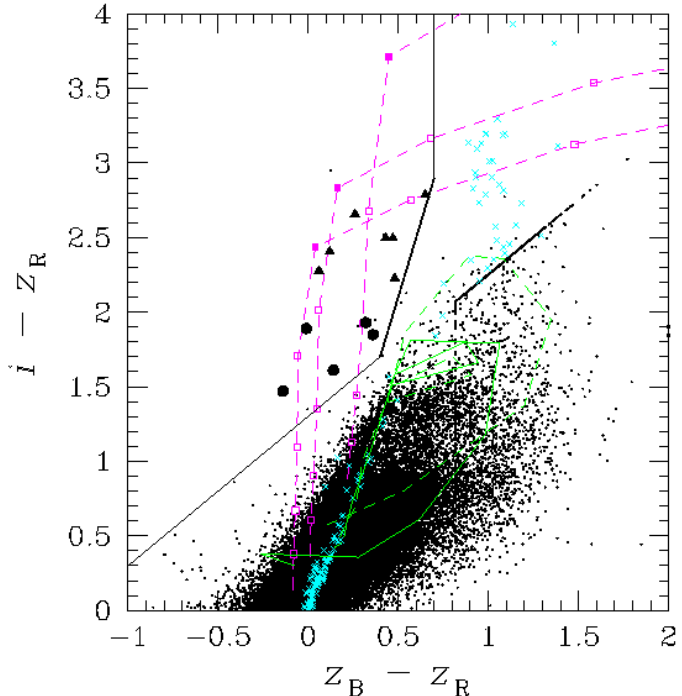


Fig. 3. Distribution of objects in the $i - z_R$ versus $z_B - z_R$ plane. The dots indicate objects detected in our data. If the i or z_B magnitude of an object is fainter than the 2σ magnitude of the corresponding bandpass, it is replaced with the 2σ magnitude. The dots along the line $i - z_R = z_B - z_R + 1.25$ at $z_B - z_R > 0.8$ are objects which are fainter than the 2σ magnitude in both i and z_B . The 12 LBG candidates are shown by filled circles (i magnitudes brighter than the 2σ mag) and filled triangles (fainter than the 2σ mag). The magenta dashed lines represent the predicted tracks of young star-forming galaxies with three different dust extinction values: from lower left to upper right, $E(B - V) = 0, 0.15, 0.5$. On the tracks, redshifts are marked by small squares with 0.2 interval; the filled squares correspond to $z = 6$. The green lines imply the tracks of elliptical galaxies redshifted from $z = 0$ to 3 without evolution; the spectra are taken from Fukugita et al. (1995; solid line) and Coleman et al. (1980; dashed line). The cyan crosses represent Galactic stars given in Gunn & Stryker (1983) and Knapp et al. (2004). The adopted boundary for LBG selection is shown by the thick solid line.

value of $E(B - V) = 0.15$ is the median extinction of $z \sim 4$ LBGs detected in the SDF (Ouchi et al. 2004a). For the intrinsic spectrum of the young galaxies, we adopt the spectral synthesis model of Kodama & Arimoto (1997) and set an age of 0.1 Gyr, Salpeter IFM, and a star-formation timescale of 5 Gyr. We use Calzetti et al.'s (2000) formula for dust extinction and Madau's (1995) prescription for the absorption by the IGM. It is found that the $i - z_R$ colors of the model galaxies increase monotonically with redshift up to $z = 6$ while their $z_B - z_R$ colors stay nearly constant. At $z > 6$, the model galaxies become rapidly redder in $z_B - z_R$.

The crosses represent 175 Galactic stars of a wide variety of types given in the spectrophotometric atlas of Gunn & Stryker (1983) and 46 Galactic cool stars taken from Knapp et al. (2004) for which spectra are available

down to 7000 Å. The green solid and green dashed curves represent the tracks of elliptical galaxies from $z = 0$ to $z = 3$ (without evolution) given in Fukugita, Shimasaku, & Ichikawa (1995) and Coleman, Wu, & Weedman (1980), respectively; these two curves are plotted to show the position and its typical uncertainty in the $i - z_R$ vs $z_B - z_R$ plane of the reddest interlopers. Coleman et al.'s spectrum does not show a UV upturn and thus has redder colors than Fukugita et al.'s.

Figure 3 demonstrates that LBGs at $z \simeq 5.6 - 6.2$ are separated well from foreground objects (intermediate-redshift red galaxies and Galactic stars) in the $i - z_R$ vs $z_B - z_R$ plane. A simple selection of LBGs using a single color, e.g., $i - z_R$, may suffer from contamination, since red galaxies at $z \sim 1 - 2$ and cool stars have similar $i - z_R$ colors to $z \sim 6$ LBGs; $z_B - z_R$ color plays an essential role in discriminating such interlopers from LBGs.

Previous two-color selections of $z \lesssim 5$ LBGs have usually adopted for the vertical axis of the two-color plane (i.e., the axis sensitive to the Lyman break) the bluest bandpass minus the middle-wavelength bandpass; for example, for B, R, i -selected LBGs at $z \sim 4$, $B - R$, not $B - i$, is adopted as the vertical axis. In this study, however, we have adopted $i - z_R$, not $i - z_B$, for the vertical axis from the technical reason that since we are based on a z_R -detected catalog, some objects are undetected in z_B , for which $i - z_B$ colors cannot be expressed properly. Of course, adopting $i - z_B$ instead of $i - z_R$ does not change our result as long as we use the same selection criteria.

From Figure 3, we define the selection criteria for LBGs at $z \sim 6$ as:

$$\begin{aligned} i - z_R &\geq z_B - z_R + 1.3, \\ z_B - z_R &\leq 0.7, \\ i - z_R &\geq 4(z_B - z_R) + 0.1, \\ B, V, R &\geq 2\sigma \text{ mag.} \end{aligned}$$

The selection boundary in the $i - z_R$ vs $z_B - z_R$ plane defined by these criteria is shown by the black solid lines in the figure. These criteria select a model galaxy with $E(B - V) = 0.15$ at $z = 5.6 - 6.2$. Varying $E(B - V)$ over 0 and 0.5 does not significantly change the redshift range selected. To further reduce contamination from foreground galaxies, we impose the fourth criterion that an LBG candidate must be un-detected, i.e., less than the 2σ limiting flux, in any of the B , V , and R images.

The dots indicate the objects detected in our data. The black circles and triangles indicate LBG candidates in our data which satisfy all the selection criteria; triangles correspond to objects not detected in i , i.e., fainter than the 2σ magnitude. All the observed magnitudes and colors have been corrected for Galactic absorption using Schlegel, Finkbeiner, & Davis (1998).

We select 12 LBG candidates in total down to $z_R = 25.4$, which are summarized in Table 2. We do not plot the error bars in Figure 3 to avoid crowding. The typical 1σ errors in $z_B - z_R$ and $i - z_R$ for the 12 candidates are 0.3 mag and 0.4 mag, respectively (The $i - z_R$ error is estimated for objects with i magnitudes brighter than the 2σ mag). The

total z_R magnitudes (MAG_AUTO) of all 12 candidates are fainter than 24.8. However, all the candidates are visible in both z_B , z , and NB921 images above the 3σ level, meaning that they are not spurious objects.

The FWHMs of the 12 candidates in the z_R image span over $0.''86 - 1.''78$, with a median of $1.''2$ and an interquartile range of $1.''14 - 1.''53$. Similar FWHM values are obtained for the z image which is considerably deeper than z_R . For most of them, the deviation from the PSF is not significant, when we consider that SExtractor tends to return FWHM values slightly larger than the PSF size for very faint point sources. Visual inspection of the 12 candidates in the z image finds that three objects seem to be resolved, with a major axis of about $2''$. The relatively large seeing size of our data prevents us from measuring the intrinsic sizes of candidates, but some brightest LBGs at $z \sim 6$ could have a large star forming region of several kpc.

Snapshots of the 12 candidates are shown in Figure 4. In this figure, the ID number increases from top to bottom, and the bandpasses are $B, V, R, i, \text{NB816}, z_B, z, \text{NB921}, z_R$ from left to right. All the objects are found to be detected clearly in both z_B , z , and NB921, while some are not visible in i or NB816, which are expected to be at higher redshifts. The sky distribution of the 12 candidates is shown in Figure 5. The dotted lines outline the region in which the LBG selection is made. The area in the lower-left corner, which corresponds in size to the field of view of a single CCD, is not used in this study, since the quantum efficiency of the CCD in charge of this area is about two thirds those of the other nine CCDs and thus the data of this area are considerably noisy.

We estimate a possible contamination rate for simple i -dropout selection. If we omit $z_B - z_R \leq 0.7$ and $i - z_R \geq 4(z_B - z_R) + 0.1$ criteria and thus select objects based on a simple i -dropout criterion ($i - z_R \geq z_B - z_R + 1.3$, similar to the criteria adopted in the previous studies) and non-detection in B, V, R , then we have ten more candidates. These newly selected ten objects might be LBGs at $z > 6.2$ or very dusty LBGs at $z < 6$, but they are more likely to be foreground objects. If all of them are really foreground objects, the contamination fraction will be $\simeq 50\%$, implying that bright single-color selected i -dropout samples for $z \sim 6$ LBGs are highly contaminated. An accurate evaluation of contamination needs spectroscopic observation of these objects. It should be, however, emphasized that the two criteria we omit in this simulation, which set an upper limit to the $z_B - z_R$ color of LBG candidates, not only reduce a possible contamination from foreground objects but also provide a sharp upper limit to the redshift range of our LBG sample.

Dickinson et al. (2004) found five $z \sim 6$ candidates in HST ACS data of the two GOODS fields based on $i - z$ color. Among them, three are brighter than $z = 25.4$, giving a surface density of $0.009 \text{ arcmin}^{-2}$. Stanway et al. (2003, 2004) made a similar i -drop survey in the same fields. There are in total nine LBG candidates with $z \leq 25.4$ in their LBG samples; the surface density

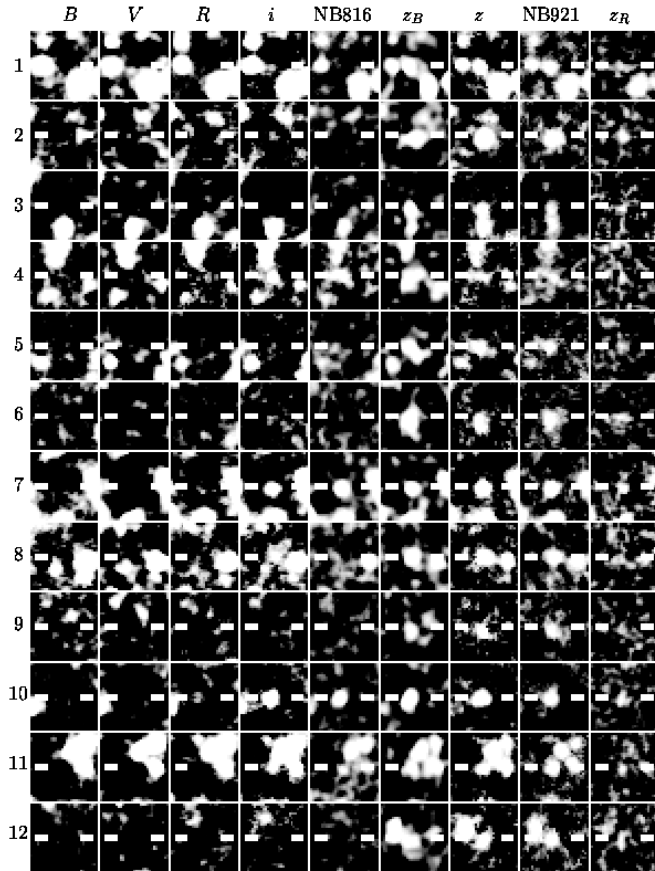


Fig. 4. Snapshots of 12 LBG candidates. From left to right, $B, V, R, i, \text{NB816}, z_B, z, \text{NB921}, z_R$ images are placed. The image size is $6''$ a side. North is up and east is to the left.

is $0.026 \text{ arcmin}^{-2}$. There is one object with $z \leq 25.4$ in Bouwens et al.'s (2003) data of the ACS Guaranteed Time Observation fields (46 arcmin^2), giving a surface density of 0.02 arcmin^{-2} . These values differ by up to a factor of two from ours, $12 \text{ candidates} / 767 \text{ arcmin}^2 = 0.016 \text{ arcmin}^{-2}$. In general, however, surface density measurements depend on selection criteria, redshift range surveyed, and detection completeness, which are different among the authors. Thus, we do not make a detailed comparison of surface density.

5. Results and Discussion

5.1. Number Density of Bright LBGs

Since the 12 LBG candidates are distributed in a narrow range of z_R magnitude, $z_R = 24.8 - 25.4$, we do not fit the Schechter function to the data to derive the best-fit values of the three Schechter parameters (α , M^* , and ϕ^*). Instead, we measure the normalization of the luminosity function ($\text{num mag}^{-1} \text{ Mpc}^{-3}$) at the average z_R magnitude of our sample ($z_R = 25.1$). This average magnitude corresponds to an rest-frame far-ultraviolet (FUV: around 1400\AA) absolute magnitude of $M_{\text{FUV}} = -21.6 \text{ mag}$ at $z = 5.9$, the central redshift of our survey. The abso-

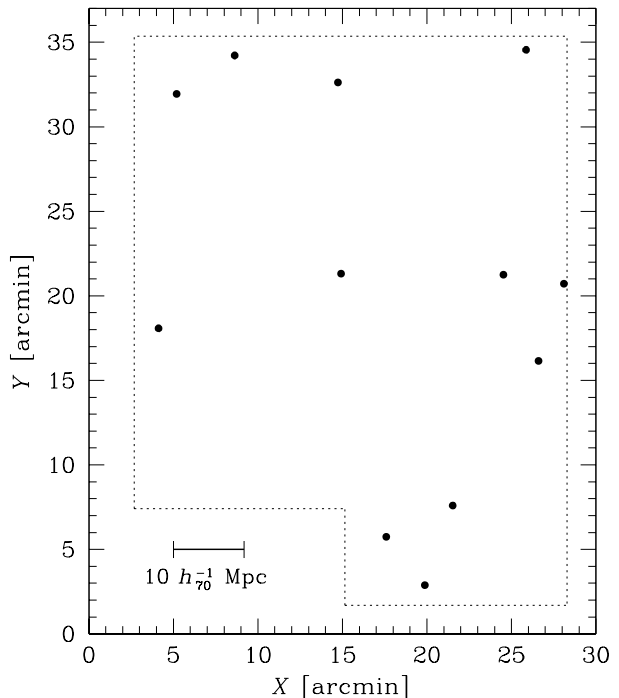


Fig. 5. Sky distribution of 12 LBG candidates. LBG selection is made in the region outlined by the dotted line.

lute magnitude is calculated as $M_{\text{FUV}} = m - 5 \log(d_L(z)) + 2.5 \log(1+z)$, where $d_L(z)$ is the luminosity distance. The rest-frame wavelength corresponding to the central wavelength of the z_R band changes from 1491\AA (at $z = 5.6$) to 1367\AA ($z = 6.2$). We assume that LBGs have flat spectra ($f_\nu = \text{const}$) over this wavelength range.

The value of the luminosity function at $M_{\text{FUV}} = -21.6$ is calculated as:

$$\phi(-21.6) [\text{mag}^{-1} \text{ Mpc}^{-3}] = \frac{1}{0.6} \times \sum_{i=1}^{12} \frac{1}{V_{\text{eff}}(m_i)} \quad (1)$$

where m_i is the z_R magnitude of the i -th candidate, $V_{\text{eff}}(m_i)$ is the effective survey volume (comoving) for the i -th candidate, and 0.6 is the size of the magnitude bin. The effective volume for a given apparent magnitude m is computed by $V_{\text{eff}}(m) = \int_z p(m, z) \frac{dV}{dz} dz$, where $p(m, z)$ is the probability that an LBG of magnitude m and redshift z is detected in our z_R image and passes the selection criteria defined above when photometric errors are taken into account (Steidel et al. 1999), and $\frac{dV}{dz}$ is the differential comoving volume for a solid angle of 767 arcmin^2 .

We estimate $p(m, z)$ assuming that the color distribution of $z \sim 6$ LBGs is similar to that of bright $z \sim 4$ LBGs detected in the SDF by Ouchi et al. (2004a) and that color differences among LBGs are due to different $E(B-V)$ values. Ouchi et al. (2004a) found that the $E(B-V)$ of $z \sim 4$ LBGs is distributed rather uniformly

over $0 \leq E(B - V) \leq 0.3$ (They adopted a single, young age for their LBGs to estimate $E(B - V)$). We generate a number of young LBGs uniformly over $0 \leq E(B - V) \leq 0.3$, assign them apparent z_R magnitudes, and distribute them randomly on the original z_R image. The value of $p(m, z)$ is calculated as the ratio of the number of simulated LBGs (with given z_R mag and redshift z) which are detected and pass the selection criteria defined above, to the total number of simulated LBGs. In this simulation, we assume that the shape of LBGs is PSF-like ($\text{FWHM} = 1''.0$). The systematic difference between input magnitudes and magnitudes measured by SExtractor is found to be negligible in our simulation. The median FWHM value of simulated objects measured by SExtractor is also found to agree with that of the 12 LBG candidates. The probability for $z_R = 25.1$, $p(25.1, z)$, is a function of redshift with a peak of 0.70 at $z = 5.9$ and a rather steep slope on both low-redshift and high-redshift sides; its FWHM is about 0.6. Hence, the relation between apparent magnitude and absolute magnitude is sufficiently tight in our sample.

We obtain $\phi(-21.6) = (2.6 \pm 0.7) \times 10^{-5} \text{ mag}^{-1} \text{ Mpc}^{-3}$, where the error indicates the Poisson error ($= 1/\sqrt{12}$). Although we have not searched for the best-fit values for the Schechter parameters, the fact that no LBG candidate is found at $z_R < 24.8$ in our data appears to favor a faint M_{FUV}^* . About four LBGs with $z_R < 24.8$ are expected to be found if we fix $\alpha = -1.6$ and $M_{\text{FUV}}^* = -21.04$, which are the values for $z \sim 3$ LBGs (ϕ^* is adjusted so that $\phi(-21.6)$ takes the correct value). Similarly, adopting $M_{\text{FUV}}^* = -20$ and -22 gives 0.7 and 9 candidates, respectively. In the previous studies, Bouwens et al. (2004a) have obtained relatively faint $M_{\text{FUV}}^* = -20.26$ from their *i*-drop sample, while Bunker et al. (2004) found that the M^* of $z \sim 6$ LBGs is consistent with the value observed at $z \sim 3$.

Bouwens et al. (2004a) derived the luminosity function of *i*-drop galaxies at $z \sim 6$ from HST ACS data of the GOODS fields and the Hubble Ultra Deep parallel fields. The normalization of the bright part ($M_{\text{FUV}} < -19.7$) of their luminosity function has been determined primarily from the wide-field ($> 300 \text{ arcmin}^2$) GOODS data. The set of the best-fit Schechter parameters they obtained is $\alpha = -1.15$, $M_{\text{FUV}}^* = -20.26$, and $\phi^* = 0.00173 \text{ Mpc}^{-3}$, which gives $\phi(-21.6) = 4.3 \times 10^{-5} \text{ Mpc}^{-3}$. This $\phi(-21.6)$ value is about 70% as high as the value obtained by us. The major portion of this difference can be accounted for by the Poisson errors in both measurements, but cosmic variance probably contributes to it to some degree. In any case, our number-density measurement must be more reliable, since it is based on wide-field two-color selection. Our survey area is larger than the sum of the two GOODS fields by more than factor two, thus being less sensitive to cosmic variance. Cosmic variance is probably higher for brighter LBGs, since observations of LBGs at $z \lesssim 5$ have revealed that brighter objects tend to be clustered more strongly (e.g., Giavalisco & Dickinson 2001; Ouchi et al. 2004b). We obtain a rough estimate of the cosmic variance following Somerville et al. (2004). The right panel of their figure 3 shows that the root variance of dark matter at $z = 6$ for our survey volume (1.1×10^6

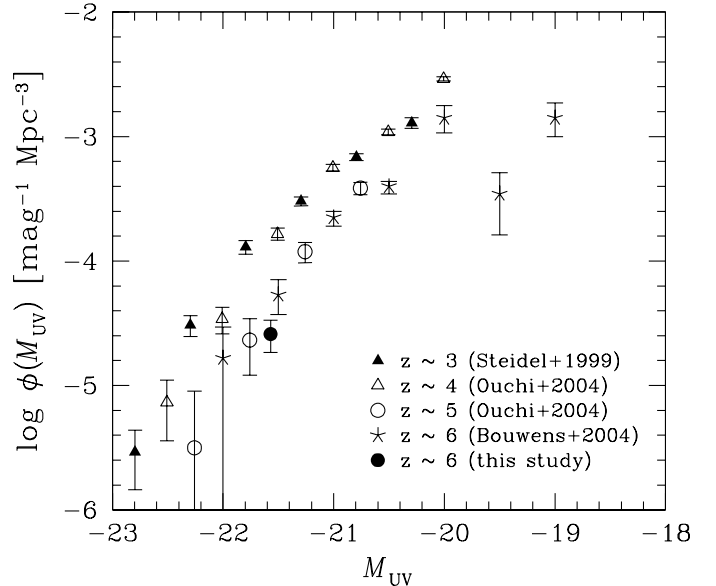


Fig. 6. FUV luminosity functions of LBGs at $z \sim 3$ (filled triangles: Steidel et al. 1999), $z \sim 4$ (open triangles: Ouchi et al. 2004a), $z \sim 5$ (open circles: Ouchi et al. 2004a), and $z \sim 6$ (stars: Bouwens et al. 2004a; filled circle: this study).

Mpc^3) is 0.033 in the $\Lambda = 0.7$ Cold Dark Matter model. Assuming a one-to-one correspondence between LBGs and dark haloes, we find from the left panel of the same figure that the bias parameter of dark haloes at $z = 6$ with the same number density as of our LBGs ($1.5 \times 10^{-5} \text{ Mpc}^{-3}$) is 7.3. The cosmic variance is thus predicted to be about 25% ($= 0.033 \times 7.3$).

We plot in Figure 6 the FUV luminosity function measurements for LBGs at $z \sim 3$ (Steidel et al. 1999), $z \sim 4$ and 5 (Ouchi et al. 2004a from shallower SDF data), and $z \sim 6$ (Bouwens et al. 2004a and this study). The number density of faint $z \sim 6$ LBGs detected in the HUDF (Yan & Windhorst 2004; Bunker et al. 2004) appears to be consistent with Bouwens et al.'s (2004a) luminosity function. We focus on bright ($M \lesssim -21$) LBGs for which our measurement is available. An interesting trend is seen that bright LBGs are less numerous at higher redshift, although the difference between $z \sim 5$ and 6 may not be so significant. The number density of bright LBGs drops by a factor of about five from $z \sim 3$ to ~ 6 .

The observed drop of the number density could be due to either dust absorption or a real decrease in LBGs. Adelberger & Steidel (2000) found no significant correlation between apparent magnitude and $E(B - V)$ for LBGs at $z \sim 3$. A similar result was obtained by Ouchi et al. (2004a) for $z \sim 4$ LBGs. These results imply that appar-

ently brighter LBGs will on average have brighter intrinsic luminosities, although there is a large scatter between intrinsic and apparent luminosities. Ouchi et al. (2004a) also found that the $E(B-V)$ distribution does not change over $z \sim 3$ and $z \sim 4$. If the dust properties found in $z \sim 3-4$ LBGs apply to $z \geq 5$ LBGs as well, then we can interpret Figure 6 as suggesting that the number density of intrinsically bright LBGs decreases with redshift. Another possibility is that the observed decline in bright LBGs is due to an increase in the dust absorption of bright LBGs with redshift; in this case, the number density of intrinsically bright LBGs may not necessarily drop with redshift. However, there is so far no observation showing evolution in dust properties of LBGs with redshift. In §5.3, we discuss the evolution of the FUV luminosity density of bright galaxies over $0 \lesssim z \lesssim 6$, assuming that the dust properties are unchanged over this redshift range.

5.2. Star Formation Rates

We calculate the star formation rates of the 12 LBG candidates from their FUV continuum luminosity using the formula given in Madau et al. (1998), which assumes a Salpeter IMF with $0.1M_{\odot} < M < 125M_{\odot}$. In the calculation, all the candidates are assumed to be located at $z = 5.9$. The results are given in Table 2. The star formation rates of the 12 candidates are found to be $\simeq 20-30 M_{\odot} \text{ yr}^{-1}$, with an average of $23 M_{\odot} \text{ yr}^{-1}$. The amount of dust extinction for the candidates cannot be estimated from our data, but if it is similar to the typical value for $z \sim 3-4$ LBGs, $E(B-V) \simeq 0.15$, then the extinction-corrected star formation rate of each candidate will be close to $1 \times 10^2 M_{\odot} \text{ yr}^{-1}$. If these candidates maintain the observed star formation rates for about 1 Gyr since $z = 6$, they will have stellar masses of $\gtrsim 3 \times 10^{10} M_{\odot}$ at $z = 3$. This value is comparable to the observed stellar masses of bright $z \sim 3$ LBGs (Papovich et al. 2001; Shapley et al. 2001).

5.3. Evolution of the FUV Luminosity Density

We measure the completeness-corrected FUV luminosity density, ρ_L , contributed from LBGs brighter than $M_{\text{FUV}} = -21.3$ as:

$$\rho_L(< -21.3) [\text{ergs s}^{-1} \text{Hz}^{-1} \text{Mpc}^{-3}] = \sum_{i=1}^{12} \frac{L(m_i)}{V_{\text{eff}}(m_i)} \quad (2)$$

where $L(m_i)$ is the FUV luminosity ($\text{ergs s}^{-1} \text{Hz}^{-1}$) corresponding to apparent magnitude m_i . The absolute magnitude $M_{\text{FUV}} = -21.3$ is close to M_{FUV}^* of $z \sim 3-4$ LBGs. We find $\rho_L(< -21.3) = (2.8 \pm 0.8) \times 10^{24} \text{ ergs s}^{-1} \text{Hz}^{-1} \text{Mpc}^{-3}$, which is equivalent to a star formation rate density of $(3.5 \pm 1.0) \times 10^{-4} M_{\odot} \text{ yr}^{-1} \text{Mpc}^{-3}$. If we integrate the luminosity function of Bouwens et al. (2004a) over $M_{\text{FUV}} < -21.3$, we obtain $6.3 \times 10^{-4} M_{\odot} \text{ yr}^{-1} \text{Mpc}^{-3}$. Stanway et al. (2003, 2004) estimated the star formation rate of $z \sim 6$ LBGs brighter than $z = 25.6$ in each of the two GOODS fields. They found $(6.7 \pm 2.7) \times 10^{-4} M_{\odot} \text{ yr}^{-1} \text{Mpc}^{-3}$ for the GOODS-South and $(5.4 \pm 2.2) \times 10^{-4} M_{\odot} \text{ yr}^{-1} \text{Mpc}^{-3}$ for the GOODS-North. These values are

higher than ours, mainly reflecting the higher number density of bright LBGs selected in the GOODS fields than in the SDF as discussed in §5.1.

As will be discussed below, our sample shows that the FUV luminosity density of bright ($M_{\text{FUV}} < -21.3$) LBGs at $z \sim 6$ is 11 times lower than that at $z \sim 3$. This ratio is reduced to 6–8 if Stanway et al.’s (2003, 2004) estimates are adopted. In the same GOODS fields, Giavalisco et al. (2004) found a factor of 3.5 decrease from $z \sim 3$ to $z \sim 6$ for $z_{850} < 26$ LBGs. The smaller decreasing factor found by Giavalisco et al. (2004) is probably due to the fainter limiting magnitude of their sample, since the evolution of FUV luminosity density tends to be milder for fainter galaxies (see below).

We examine how the luminosity densities for bright galaxies and all galaxies evolve over $0 \leq z \leq 6$, and whether or not there is a remarkable difference in their evolutionary behavior. Figure 7 shows the observed evolution of FUV luminosity density over $0 \leq z \leq 6$. The large symbols indicate the luminosity density contributed from bright ($M_{\text{FUV}} < -21.3$) galaxies, $\rho_L(< -21.3)$, while the small symbols are for the luminosity density from galaxies down to a faint limit of $M_{\text{FUV}} = -19.0$, $\rho_L(< -19.0)$. We use $\rho_L(< -19.0)$ as a substitute for the total FUV luminosity density in the universe, assuming that $\rho_L(< -19.0)$ traces the relative change in the total luminosity density acceptably, although the contribution from galaxies fainter than -19 mag is uncertain and may be considerably large. The filled circle indicates our measurement, while the other kinds of symbols represent previous measurements taken from the literature. We use Bouwens et al.’s (2004a) luminosity function to calculate $\rho_L(< -19.0)$ at $z = 6$. The vertical axis on the right-hand side of Figure 7 shows corresponding star formation rate density. Dust extinction correction has not been applied to any measurements. The star formation rate density calculated from $\rho_L(< -19.0)$ multiplied with factor 10 is roughly consistent with recent measurements of the extinction-corrected total star formation rate density (Hopkins 2004).

We find that $\rho_L(< -21.3)$ evolves drastically with redshift. It increases by an order of magnitude from $z \sim 6$ to ~ 3 , has a rather sharp peak at $z \sim 3$, and then drops by (more than) three orders of magnitude to the present epoch. The evolution of $\rho_L(< -19.0)$, on the other hand, is much milder. Over $1 \leq z \leq 6$, $\rho_L(< -19.0)$ is roughly constant within a factor of about five, and then it decreases by ten times from $z \sim 1$ to the present epoch. As a result, $\rho_L(< -21.3)/\rho_L(< -19.0)$ reaches a maximum around $z = 3$.

The remarkably different evolution of $\rho_L(< -21.3)$ and $\rho_L(< -19.0)$ probably reflects a change in M_{FUV}^* with time. It has been found that M_{FUV}^* fades by 3 magnitude from $z = 3$ ($\simeq -21$) to $z = 0$ ($\simeq -18$) (Arnouts et al. 2005). A faint M_{FUV}^* is suggested for $z \sim 6$ LBGs since no candidate brighter than $z_{\text{R}} = 24.8$ is detected. Since $M_{\text{FUV}} = -21.3$ is comparable to or brighter than M_{FUV}^* at any redshift, the luminosity function has always a sharp, exponential shape around $M_{\text{FUV}} = -21.3$. Thus, $\rho_L(< -21.3)$ is much more sensitive to the change in M_{FUV}^*

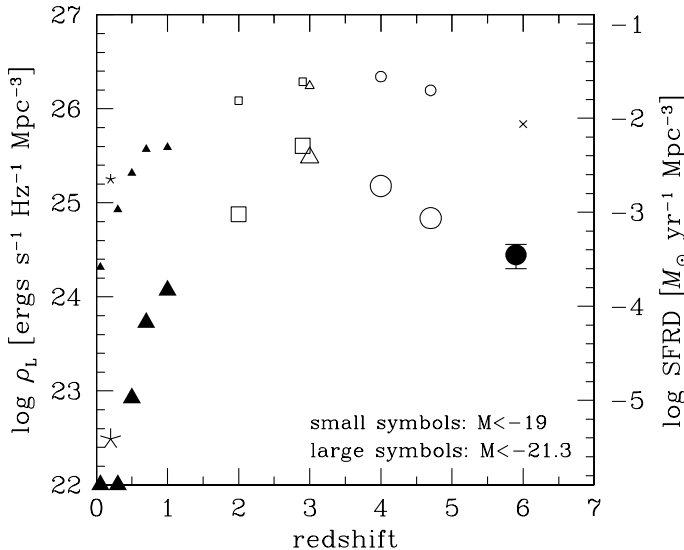


Fig. 7. Evolution of the FUV luminosity density. The large and small symbols indicate the luminosity density contributed from galaxies brighter than $M_{\text{FUV}} = -21.3$ and $M_{\text{FUV}} = -19.0$, respectively. The filled circle with error bars show our measurement, and the other symbols indicate data taken from the literature: cross: Bouwens et al. (2004a), open circles: Ouchi et al. (2004a), open triangles: Steidel et al. (1999), open squares: Arnouts et al. (2005; HDF), filled triangles: Arnouts et al. (2005; GALEX), stars: Sullivan et al. (2000). The two filled triangles at the bottom imply that the actual measurements are lower than 1×10^{22} ergs $\text{s}^{-1} \text{Hz}^{-1} \text{Mpc}^{-3}$.

than $\rho_L(< -19.0)$.

An absolute magnitude of $M_{\text{FUV}} = -21.3$ corresponds to a relatively high star formation rate of $18 M_{\odot} \text{yr}^{-1}$ (or a dust-corrected value of $80 M_{\odot} \text{yr}^{-1}$ if $E(B-V) = 0.15$ is assumed). Figure 7 shows that such actively star forming galaxies become abundant in a short cosmic time from $z = 6$ to 3 (about 1.2 Gyr) and then disappeared by the present time. Their contribution to the cosmic star formation was the highest at $z \sim 3$.

The drastic evolution of actively star forming galaxies (i.e., bright LBGs) found here may be physically interpreted as a combination of two competing processes in a Cold Dark Matter universe: the build-up of massive dark haloes with time and the decrease in the star formation rate per unit dark matter mass (i.e., specific star formation rate) in dark haloes with time. Hernquist & Springel (2003) and Springel & Hernquist (2003) have made essentially the same discussion to explain the observed cosmic star formation history.

Clustering analyses of $z \sim 3 - 5$ LBGs have shown that dark haloes hosting bright $z \sim 3 - 5$ LBGs have a total mass of $M_{\text{tot}} \sim 10^{12} M_{\odot}$ (e.g., Giavalisco & Dickinson 2001; Moustakas & Somerville 2002; Ouchi et al. 2004b). Let us assume that bright $z \sim 6$ LBGs also reside in $\sim 10^{12} M_{\odot}$ dark haloes. According to the standard Cold Dark Matter model with $\Omega_0 = 0.3$, $\lambda_0 = 0.7$, $h = 0.7$, and $\sigma_8 = 0.9$, the fraction of matter in the universe confined in dark haloes with $M_{\text{tot}} \geq 10^{12} M_{\odot}$ increases by an order of magnitude from $z = 6$ to 3 . This is similar to the observed evolution rate in the luminosity density of bright LBGs. Note that the model predicts the fraction of matter in $M_{\text{tot}} \geq 10^{12} M_{\odot}$ haloes to increase by an order of magnitude from $z = 3$ to 0 ; the increase per unit cosmic time is thus more gradual at $z < 3$ than at $3 < z < 6$.

The decrease with time in the specific star formation rate may also be qualitatively in accord with Cold Dark Matter models. Dark haloes formed later have a lower mass density, since the average mass density within dark haloes formed at a given cosmic time is proportional to the average mass density of the universe at that time. It is reasonable to expect that specific star formation rate correlates positively with the mean mass density within dark haloes. Hernquist & Springel (2003) and Springel & Hernquist (2003) have shown that gas cooling becomes insufficient in dark haloes formed at lower redshifts because of the decline of the mass density, and thus the specific star formation rate in dark haloes declines with time. They found that in their numerical simulations the cosmic star formation rate has a peak at $z \sim 5 - 6$. There may be, of course, other mechanisms which suppress star formation in haloes formed recently, such as the truncation of star formation in galaxies infalling into galaxy groups and clusters which become abundant with time, and the decrease in galaxy merging involving star formation.

If we adopt this interpretation, the observed evolution of actively star forming galaxies implies that the specific star formation rate of massive ($M_{\text{tot}} \sim 10^{12} M_{\odot}$) dark haloes is roughly unchanged over $3 \lesssim z \lesssim 6$, while it drops drastically with time at $z \lesssim 3$ for some reason, resulting in the star formation activity of the whole massive haloes being the highest around $z = 3$. The mild evolution of the total luminosity density over $z \sim 3$ and 6 looks reasonable, since the dark-matter mass summed over all haloes increases by only a factor of two or so from $z = 6$ to 3 . On the other hand, the mild evolution at $z \lesssim 3$ may be due to a gradual decrease, for some reason, in the specific star formation rate in less massive haloes.

Finally, we point out an interesting resemblance of the evolution of bright LBGs (i.e., FUV-selected actively star-forming galaxies brighter than -21.3 mag) to that of luminous dusty star-forming galaxies (submm galaxies) and QSOs. Chapman et al. (2003, 2004, 2005) found that the space density of luminous dusty star-forming galaxies increased by about an order of magnitude from $z \sim 4$ to $z \sim 2$ and then decreased by $\sim 10^3$ from $z \sim 2$ to the present time, having a sharp peak at $z \simeq 2.2$. Chapman et al. (2003) have pointed out that luminous dusty star-forming galaxies coexist with the peak activity of QSOs.

Recent wide-field QSO surveys have measured accurately the luminosity function of bright QSOs at $z \lesssim 6$, finding that the space density of bright ($M_{\text{FUV}} < -26.7$) QSOs increases by more than an order of magnitude from $z \sim 6$ to ~ 3 , shows a maximum around $z = 2.5$, and then drops by about 10^3 by the present epoch (Croom et al. 2004; Fan et al. 2001, 2004).

These three populations appear to be related with active star formation or massive galaxy formation. Dusty star-forming galaxies, detected in submillimeter or radio observations, have star formation rates of as high as $\sim 10^3 M_{\odot} \text{ yr}^{-1}$ (e.g., Chapman et al. 2003, 2004). It is widely believed that QSOs are the result of gas accretion onto a supermassive black hole at the center of a galaxy, and hence are likely be linked to active star formation in the galaxy and, possibly, to bulge formation (Franceschini et al. 1999). Nearby luminous QSOs are hosted by massive bulge-dominated galaxies (e.g., Floyd et al. 2004). It has also been found that the host galaxies of luminous QSOs at $1 < z < 2$ are consistent with massive galaxies following passive evolution (e.g., Falomo et al. 2004).

At $z \sim 2 - 3$, the number density of bright LBGs, $\sim 10^{-4} \text{ Mpc}^{-3}$, is higher than those of dusty star-forming galaxies ($\sim 10^{-5} \text{ Mpc}^{-3}$) and QSOs ($\sim 10^{-7} \text{ Mpc}^{-3}$). This may imply either that the lifetime of bright LBGs, i.e., the duration of star formation of $\gtrsim 20 - 30 M_{\odot} \text{ yr}^{-1}$, is longer than the lifetimes of dusty star-forming phase and QSO phase, or that bright LBGs reside in less massive (thus more numerous) dark haloes than the other two populations, or both. A weak clustering of $z \sim 3$ LBGs compared with the clustering of QSOs (Croom et al. 2005) and dusty star-forming galaxies (Blain et al. 2004) at similar redshifts could imply that LBGs reside in the least massive (but still as massive as $\sim 10^{12} M_{\odot}$) dark haloes. The relatively milder evolution in number density at $z > 2$ for LBGs than for dusty star-forming galaxies may also suggest smaller dark halo masses of LBGs. It is also interesting to note that the peak redshift for bright LBGs ($z \sim 3$) is slightly higher than those for dusty star-forming galaxies and QSOs ($z \sim 2 - 2.5$); this might reflect hierarchical evolution of haloes that less massive haloes are formed earlier.

The physical relationship between the three populations is not yet clear, but the resemblance of their evolution suggests that $z \sim 3$ is a remarkable era in the cosmic history when massive galaxies were being intensively formed. The cosmic time of $z \sim 3$ also falls in the suggested formation epoch of massive early-type galaxies seen at $0 \leq z \lesssim 2$ (e.g., Bower, Lucey, & Ellis 1992; Kodama et al. 1998; Stanford et al. 1998; van Dokkum & Stanford 2003; Cimatti et al. 2004; McCarthy et al. 2004).

6. Conclusions

We showed that LBGs at $z \sim 6$ are isolated well from red galaxies at $z \sim 1 - 2$ and Galactic cool stars in the $i - z_{\text{R}}$ vs $z_{\text{B}} - z_{\text{R}}$ plane. We applied this two-color selection to wide-field (767 arcmin^2) multicolor data of the Subaru Deep Field, selecting 12 candidates for $z \simeq 5.9 \pm 0.3$ LBGs down

to $z_{\text{R}} = 25.4$. This is the most reliable sample of bright $z \sim 6$ LBGs, which is robust against both contamination by foreground objects and cosmic variance.

The average star formation rate of the 12 candidates is $23 M_{\odot} \text{ yr}^{-1}$ if dust extinction is not corrected. We calculated the normalization of the rest-frame far-ultraviolet (FUV: $\simeq 1400\text{\AA}$) luminosity function of $z \sim 6$ LBGs at $M_{\text{FUV}} = -21.6$ to be $\phi(-21.6) = (2.6 \pm 0.7) \times 10^{-5} \text{ mag}^{-1} \text{ Mpc}^{-3}$. The FUV luminosity density contributed from LBGs brighter than $M_{\text{FUV}} = -21.3$ is $(2.8 \pm 0.8) \times 10^{24} \text{ ergs s}^{-1} \text{ Hz}^{-1} \text{ Mpc}^{-3}$ after correction for detection completeness, which corresponds to a star formation rate density of $(3.5 \pm 1.0) \times 10^{-4} M_{\odot} \text{ yr}^{-1} \text{ Mpc}^{-3}$.

We examined the evolution of the FUV luminosity density, or equivalently the star formation rate density, over $0 \leq z \leq 6$ by combining our measurement with those taken from the literature. We found that the FUV luminosity density for bright FUV galaxies with $M_{\text{FUV}} < -21.3$, i.e., actively star-forming galaxies, increases by an order of magnitude from $z \sim 6$ to ~ 3 and takes a rather sharp peak at $z \sim 3$, followed by 10^3 times decrease toward $z = 0$. On the other hand, the evolution of the ‘total’ luminosity density was found to be much milder. As a result, the contribution to the cosmic star formation from actively star-forming galaxies is the highest at $z \sim 3$. The drastic evolution of actively star-forming galaxies can be explained by a combination of the build-up of massive dark haloes with time and the decrease in the specific star formation rate in dark haloes with time. We also pointed out a resemblance between the evolution of bright LBGs, luminous dusty star-forming galaxies, and bright QSOs. The redshift of $z \sim 3$ seems to be a remarkable era in the cosmic history in terms of the formation of massive galaxies.

We thank the anonymous referee for useful comments which have significantly improved the paper. We are grateful to the Subaru Telescope staff for their help in the observations. M. Ouchi has been supported by the Hubble Fellowship program through grant HF-01176.01-A awarded by the Space Telescope Science Institute, which is operated by the Association of Universities for Research in Astronomy, Inc. under NASA contract NAS 5-26555.

References

- Adelberger, K. L., & Steidel, C. C. 2000, *ApJ*, 544, 218
- Ando, M. et al. 2004, *ApJ*, 610, 635
- Arnouts, S. et al. 2005, *ApJ*, 619, L43
- Bertin, E., & Arnouts, S. 1996, *A&AS*, 117, 393
- Blain, A. W., Chapman, S. C., Smail, I., & Ivison, R. 2004, *ApJ*, 611, 725
- Bohlin, R. C., Colina, L., & Finley, D. S. 1995, *AJ*, 110, 1316
- Bouwens, R. J. et al. 2003, *ApJ*, 595, 589
- Bouwens, R. J. et al. 2004a, *ApJ*, 606, L25
- Bouwens, R. J., Illingworth, G. D., Blakeslee, J. P., Broadhurst, T. J., & Franx, M. 2004b, *ApJ*, 611, L1
- Bower, R. G., Lucey, J. R., & Ellis, R. S. 1992, *MNRAS*, 254, 601

- Bremer, M. N., Lehnert, M. D., Waddington, I., Hardcastle, M. J., Boyce, P. J., & Phillipps, S. 2004, *MNRAS*, 347, L7
- Bunker, A. J., Stanway, E. R., Ellis, R. S., & McMahon, R. G. 2004, *MNRAS*, 355, 374
- Calzetti, D., Armus, L., Bohlin, R. C., Kinney, A. L., Koornneef, J., Storchi-Bergmann, T. 2000, *ApJ*, 533, 682
- Chapman, S. C., Blain, A. W., Ivison, R. J., & Smail, I. R. 2003, *Nature*, 422, 695
- Chapman, S. C., Smail, I., Blain, A. W., & Ivison, R. J. 2004, *ApJ*, 614, 671
- Chapman, S. C., Blain, A. W., Smail, I. R., & Ivison, R. J. 2005, *ApJ*, 622, 772
- Coleman, G. D., Wu, C.-C., & Weedman, D. W. 1980, *ApJS*, 43, 393
- Croom, S. M., Smith, R. J., Boyle, B. J., Shanks, T., Miller, L., Outram, P. J., & Loring, N. S. 2004, *MNRAS*, 349, 1397
- Croom, S. M. et al. 2005, *MNRAS*, 356, 415
- Dickinson, M. et al. 2004, *ApJ*, 600, L99
- Falomo, R., Kotilainen, J. K., Pagani, C., Scarpa, R., Treves, A. 2004, *ApJ*, 604, 495
- Fan, X., et al. 2001, *AJ*, 121, 54
- Fan, X., et al. 2004, *AJ*, 128, 515
- Floyd, D. J. E. et al. 2004, *MNRAS*, 355, 196
- Fontana, A. et al. 2003, *ApJ*, 587, 544
- Foucaud, S. et al. 2003, *A&A*, 409, 835
- Franceschini, A., Hasinger, G., Miyaji, T., & Malquori, D. 1999, *MNRAS*, 310, L5
- Fukugita, M., Shimasaku, K., & Ichikawa, T. 1995, *PASP*, 107, 945
- Giavalisco, M. & Dickinson, M. 2001, *ApJ*, 550, 177
- Giavalisco, M. et al. 2004, *ApJ*, 600, L103
- Gunn, J. E., & Stryker, L. L. 1983, *ApJS*, 52, 121
- Hernquist, L., & Springel, V. 2003, *MNRAS*, 341, 1253
- Hopkins, A. M. 2004, *ApJ*, 615, 209
- Hu, E. M., Cowie, L. L., Capak, P., McMahon, R. G., Hayashino, T., & Komiyama, Y. 2004, *AJ*, 127, 563
- Iwata, I. et al. 2003, *PASJ*, 55, 415
- Kashikawa, N. et al. 2004, *PASJ*, 56, 1011
- Knapp, G. R. et al. 2004, *AJ*, 127, 3553
- Kodama, T., & Arimoto, N. 1997, *A&A*, 320, 41
- Kodama, T., & Arimoto, N., Barger, A. J., & Aragón-Salamanca, A. 1998, *A&A*, 334, 99
- Madau, P. 1995, *ApJ*, 441, 18
- Madau, P., Pozzetti, L., & Dickinson, M. 1998, *ApJ*, 498, 106
- Maihara, T. et al. 2001, *PASJ*, 53, 25
- McCarthy, P. J. et al. 2004, *ApJ*, 614, L9
- Miyazaki, S., et al. 2002, *PASJ*, 54, 833
- Moustakas, L. A., & Somerville, R. S. 2002, *ApJ*, 577, 1
- Nagao, T. et al. 2004, *ApJ*, 613, L9
- Ouchi, M. 2003, Ph.D. thesis, University of Tokyo
- Ouchi, M. et al. 2004a, *ApJ*, 611, 660
- Ouchi, M. et al. 2004b, *ApJ*, 611, 685
- Ouchi, M. et al. 2005, *ApJ*, 620, L1
- Papovich, C., Dickinson, M., & Ferguson, H. C. 2001, *ApJ*, 559, 620
- Porciani, C., & Giavalisco, M. 2002, *ApJ*, 565, 24
- Schlegel, D. J., Finkbeiner, D. P., & Davis, M. 1998, *ApJ*, 500, 525
- Shapley, A. E., Steidel, C. C., Adelberger, K. L., Dickinson, M., Giavalisco, M., & Pettini, M. 2001, *ApJ*, 562, 95
- Shapley, A. E., Steidel, C. C., Pettini, M., & Adelberger, K. L. 2003, *ApJ*, 588, 65
- Shimasaku, K. et al. 2003, *ApJ*, 586, L111
- Shimasaku, K. et al. 2004, *ApJ*, 605, L93
- Somerville, R. S., Lee, K., Ferguson, H. C., Gardner, J. P., Moustakas, L. A., & Giavalisco, M. 2004, *ApJ*, 600, L171
- Springel, V., & Hernquist, L. 2003, *MNRAS*, 339, 312
- Stanford, S. A., Eisenhardt, P. R., & Dickinson, M. 1998, *ApJ*, 492, 461
- Stanway, E. R., Bunker, A. J., & McMahon, R. G. 2003, *MNRAS*, 342, 439
- Stanway, E. R., Bunker, A. J., McMahon, R. G., Ellis, R. S., Treu, T., & McCarthy, P. J. 2004, *ApJ*, 607, 704
- Steidel, C. C., Adelberger, K. L., Giavalisco, M., Dickinson, M., & Pettini, M. 1999, *ApJ*, 519, 1
- Sullivan, M., Treyer, M. A., Ellis, R. S., Bridges, T. J., Milliard, B., & Donas, J. 2000, *MNRAS*, 312, 442
- van Dokkum, P. G., & Stanford, S. A. 2003, *ApJ*, 585, 78
- Yagi, M., Kashikawa, N., Sekiguchi, M., Doi, M., Yasuda, N., Shimasaku, K., & Okamura, S. 2002, *AJ*, 123, 66
- Yan, H., Windhorst, R. A., & Cohen, S. H. 2003, *ApJ*, 585, L93
- Yan, H. & Windhorst, R. A. 2004, *ApJ*, 612, L93

Table 2. Photometric properties of LBG candidates.

ID	α (J2000.0)			δ (J2000.0)			z_R	$z_B - z_R$	$i - z_R$	NB816	z	NB921	SFR ^(a)
1	13	23	46.55	+27	27	3.9	24.84	0.12	2.41	27.04	25.96	25.88	29.2
2	13	25	27.81	+27	28	58.9	24.92	0.65	2.79	27.04	25.42	25.37	27.1
3	13	24	39.15	+27	32	13.0	24.94	0.47	2.50	27.04	26.06	26.42	26.6
4	13	23	49.72	+27	45	27.4	25.02	-0.14	1.47	26.10	26.57	26.07	24.7
5	13	24	16.91	+27	13	48.3	25.04	0.06	2.28	27.04	26.01	26.16	24.2
6	13	25	23.15	+27	42	51.1	25.14	0.26	2.66	27.04	26.24	25.76	22.1
7	13	24	9.43	+27	18	30.4	25.15	0.36	1.85	25.75	25.55	25.42	21.9
8	13	23	39.77	+27	31	37.4	25.16	-0.01	1.89	27.04	25.49	25.68	21.7
9	13	24	27.13	+27	16	40.1	25.23	0.48	2.22	27.04	26.13	25.95	20.4
10	13	23	55.87	+27	32	9.3	25.26	0.14	1.61	26.05	25.73	25.94	19.8
11	13	24	40.01	+27	43	32.3	25.36	0.32	1.93	26.95	26.19	25.87	18.1
12	13	25	7.62	+27	45	7.4	25.36	0.43	2.49	27.04	25.99	25.83	18.1